Bio-Design and Manufacturing (2025) 8:595–608
https://doi.org/10.1631/bdm.2400351

RESEARCH ARTICLE

Integrating three-dimensional printing and bioprinting technologies to develop a stretchable in vitro model of the human airway

Junned Chan[1,2,3] · Julian Gonzalez Rubio[3] · Oscar O'Dwyer Lancaster-Jones[2] · Yashasvi Verma[1] · Charlotte Büchter[4] · Stefan Jockenhoevel[3] · Laura De Laporte[1,5,6] · Mirko Trilling[7,8] · Anja Lena Thiebes[3] · Daniela Duarte Campos[1,2]

Received: 2 September 2024 / Accepted: 12 January 2025 / Published online: 27 June 2025

Abstract

The global demand for in vitro respiratory airway models has surged due to the coronavirus disease 2019 (COVID-19) pandemic. Current state-of-the-art models use polymer membranes to separate epithelial cells from other cell types, creating a nonphysiological barrier. In this study, we applied three-dimensional (3D) printing and bioprinting to develop an in vitro model where endothelial and epithelial cells were in direct contact, mimicking their natural arrangement. This proof-of-concept model includes a culture chamber, with an endothelial bioink printed and perfused through an epithelial channel. *In silico* simulations of the air velocity within the channel revealed shear stress values ranging from 0.13 to 0.39 Pa, aligning with the desired in vivo shear stress observed in the bronchi regions (0.1–0.4 Pa). Biomechanical movements during resting breathing were mimicked by incorporating a textile mesh positioned away from the cell–cell interface. The epithelial channel demonstrated a capacity for compression and expansion of up to −14.7% and +6.4%, respectively. Microscopic images showed that the epithelial cells formed a uniform monolayer within the lumen of the channel close to the bioprinted endothelial cells. Our novel model offers a valuable tool for future research into respiratory diseases and potential treatments under conditions closely mimicking those in the lung.

Junned Chan and Julian Gonzalez Rubio have contributed equally to this work.

✉ Daniela Duarte Campos
dcampos@uni-heidelberg.de

[1] Advanced Materials for Biomedicine (AMB), Institute of Applied Medical Engineering (AME), Center for Biohybrid Medical Systems (CBMS), University Hospital RWTH Aachen, Aachen 52074, Germany

[2] Bioprinting & Tissue Engineering, Center for Molecular Biology of Heidelberg University (ZMBH), Heidelberg 69120, Germany

[3] Biohybrid & Medical Textiles (BioTex), Institute of Applied Medical Engineering (AME), Helmholtz Institute for Biomedical Engineering, RWTH Aachen University, Aachen 52074, Germany

[4] ITA Institute for Textile Technology, RWTH Aachen University, Aachen 52074, Germany

[5] DWI – Leibniz Institute for Interactive Materials, Aachen 52074, Germany

[6] Institute of Technical and Macromolecular Chemistry (ITMC), RWTH Aachen University, Aachen 52074, Germany

[7] Institute for Virology, University Hospital Essen, University of Duisburg-Essen, Essen 45147, Germany

[8] Institute for the Research on HIV & AIDS-associated Diseases, University Hospital Essen, University of Duisburg-Essen, Essen 45147, Germany

Graphical abstract

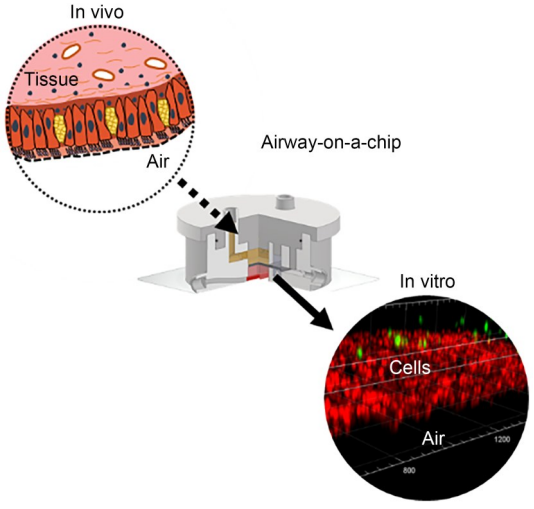

Keywords Airway-on-a-chip · In vitro model · Bioprinting · Hydrogel · Tissue engineering · Lung

1 Introduction

Respiratory diseases continue to pose a significant public health challenge, with the advent of severe acute respiratory syndrome coronavirus 2 (SARS-CoV-2), highlighting the need for innovative technologies and effective therapies. Traditional approaches for studying diseases, such as two-dimensional (2D) cell cultures and animal models, have significant limitations in mimicking complex cellular microenvironments or accurately mimicking the properties of human tissues and organs. Moreover, animal models often yield misleading results due to species-specific differences in physiological structures and tissue and organ functions [1, 2]. In addition to ethical and legal concerns, animal models are time-consuming and costly [3]. Consequently, their use is increasingly unsuitable for meeting the growing demands of drug testing. A novel approach using tissue-on-chips has emerged.

Tissue-on-chips integrate the advantages of microfluidic technologies and three-dimensional (3D) cell culturing. These biomimetic experimental platforms are designed to mimic the physiology and functions of human organs and tissues in a reductionist manner. A distinguishing feature is the precise control of fluids and particles, typically within channels and chambers at the microliter scale [4–6]. This attribute facilitates the control of biomolecule concentrations and fluid flow rates, offering enhanced replication of the physiological conditions present within complex tissues [7, 8]. On-chip devices are predominantly fabricated using lithography techniques with polydimethylsiloxane (PDMS) [5, 9], an optically transparent, highly biocompatible silicon-based elastomer [9]. The chambers cast inside the chip enable cells to grow and expand in all dimensions, mimicking their natural biological behavior and environment.

Most state-of-the-art airway-on-a-chip (AoC) devices are designed to mimic an air–liquid interface (ALI) to mimic the morphology and functionality of airways [10]. Such interfaces are commonly created using a cell-seeded PDMS membrane separating two chambers, with the basal side exposed to a recreated internal microenvironment and the apical side in contact with air [11]. In addition to cellular composition and physiological interfaces, it is essential to incorporate physiologically relevant biomechanical stimuli into in vitro testing platforms. Conducting in vitro assays using only static models, such as 2D cell cultures, may yield misleading results if mechanical forces and fluid flow rates are not adequately considered [3, 12]. An active dynamic interface is essential for mimicking living organs and tissues [12, 13]. Stimuli, such as wall shear stress, are often introduced through the perfusion of fluids within the chip [14]. Furthermore, dynamic stimuli similar to those found in native airway tissue can be mimicked by applying physical forces to the flexible polymer membrane in the ALI, as described in the chip design by Huh et al. In this device, a stretch motion is initiated by applying a vacuum to the side chambers of the chip, which are connected to the ends of the membranes [12].

Compared to traditional models, on-chip technology offers superior cost-effectiveness, efficiency, and accuracy in mimicking tissue physiology. Despite these advantages,

challenges remain in state-of-the-art chips, such as production time, complexity, and reproducibility [15]. Another concern is the widespread use of relatively rigid polymeric surfaces, such as PDMS or polyethylene terephthalate (PET), respectively, in fluidic devices and airway model membranes. A major disadvantage of using commercially available PET membranes is their lack of flexibility [16], a crucial characteristic for developing a dynamic AoC. Conversely, PDMS offers high elasticity and optical transparency; however, it requires a prolonged curing time and extensive manual handling, limiting automation and reducing manufacturing throughput efficiency [16, 17]. This hinders the industrial applicability of the process and material. Another significant issue is the sensitivity of certain materials to hydrophobic molecules present in fluorescent dyes, chemical compounds, and drugs, which may confound drug assays [9, 18, 19]. Furthermore, incomplete polymerization of these materials can contaminate culture media with prepolymer, potentially affecting cell behavior [20]. Although PDMS-based fluidic devices are ideal for prototyping, their application in drug-testing assays is limited. Most fluidic chips are built on a micron scale, which restricts the volume of the tested model and consequently limits the density of seeded cells. Hence, conventional biochemical assays often fail to produce statistically significant data [21]. Overall, these limitations must be considered when selecting materials and designing robust fluidic systems with broad industrial applicability.

The criteria for fabricating a new engineered AoC, including fabrication methods, material, design, and device specifications, have been compiled and listed (Table 1).

Before designing a newly engineered AoC, a comprehensive comparison of features, strengths, and limitations was conducted, evaluating state-of-the-art models alongside the proposed design (Table 2).

This study presents the development of a novel 3D-printed, stretchable AoC device designed to mimic the mechanical stimulation and dynamic fluid flow of native airways (Fig. 1). By adopting alternative manufacturing techniques and materials, the challenges associated with

Table 1 Requirements for fabricating an AoC

Requirements for fabrication methods	Description
Rapid prototyping and fabrication	The fabrication process must minimize the design-to-product cycle and eliminate complex material handling. It must support the production of complex geometries with minimal steps, ideally enabling one-step device fabrication.
Reproducibility	The device must be reproducible for consistent manufacturing.
Ease of scaling for mass production	The chosen fabrication method should easily transition from prototype development to mass production.
Cost-effective fabrication	The fabrication strategy must be economical for both small-scale research batches and large-scale commercial production.
Requirements for material	**Description**
Biocompatibility and nontoxicity	The device must be fabricated from biocompatible and nontoxic materials.
Availability and affordability	Materials utilized should be accessible and inexpensive.
Alternative to PDMS	A PDMS-free design reduces the risk of interference in drug assays and provides better scalability for industrial applications.
Ease of sterilization	Materials should be easy to clean and sterilize to prevent contamination during operation or reuse.
Optical transparency	Materials should maintain optical clarity, ensuring minimal obstruction for analysis resulting from opacity.
Requirements for design	**Description**
Interface establishment	The design must enable forming a functional cell interface and an ALI.
Functionality channels	The design should integrate channels for efficient fluid supply and removal.
Functionality chambers	The design must include functional chambers for cell culture and extracellular matrix (ECM) stabilization.
Compression element integration	The design must include features for integrating functional elements to apply compression at the cell interface.
Real-time monitoring	The design must support real-time analysis of the cell interface and culture.
Connectivity	The device must include components for seamless integration with external systems, such as pumps.
Bioprinting compatibility	The design should be compatible with bioprinting technologies.
Requirements for device	**Description**
Compression capability	The device must support ALI compression without compromising structural integrity.
Ease of handling	The device should be ergonomically designed for user-friendly operation.

Table 2 Comparison of key features, strengths, and limitations of state-of-the-art in vitro airway models and the proposed engineered AoC

Model	Features	Strengths	Limitations
Nawroth et al.'s [22]	Mimicking breathing mechanics through combined mechanical stretching and directional flow	· Integrating dynamic flow and mechanical stretch · Improved cellular function	· Using PDMS as a fabrication material · Reduced cell–ECM interactions due to cells grown on an ECM-coated membrane · Complex implementation
Huh et al.'s [12]	Recreating the alveolar–capillary interface with integrated cyclic mechanical strain and ALI	· Integrating dynamic flow and mechanical stretch · Improved cellular function	· Using PDMS as a fabrication material · Reduced cell–ECM interactions due to cells grown on an ECM-coated membrane
Sakolish et al.'s [23]	Long-term coculture system for small-airway epithelial and endothelial cells under ALI, exposed to toxic environments	· Mimicking ALI · Supporting long-term physiological maintenance of airway epithelium · Cost-effective	· Using PDMS as a fabrication material · Lacking mechanical stimulation · Lacking multicellular tissue architecture · Low throughput · Open inlet design
Zhu et al.'s [24]	Mimicking alveolar expansion and contraction using regular airflow to induce deformation	· Integrating cyclic stretching · Enabling innovative real-time monitoring	· Complex design · Using PDMS as a fabrication material · Lacking multi-tissue architecture · Scalability restriction
Park et al.'s [25]	Airway chip with bidirectional airflow, enabling glycocalyx formation	· Integrating bidirectional airflow to simulate breathing and mucociliary clearance	· Lacking mechanical stimulation · Simplified design with limited ECM complexity, as cells are cultured on a matrix-derived membrane
Our approach	Mimicking airway functionality with mechanical stimulation and dynamic fluid flow and incorporating bioprinting and 3D polymer printing	· PDMS-free design · Integrating mechanical stretching at a distance from the cell interface · Integrating membrane-free design, allowing direct cell–cell interactions · Enhanced optical accessibility regardless of chip material · Supporting real-time analysis of the cell interface · Customizable and scalable through additive manufacturing technologies	· Requiring manual strain induction · Early development stage · Limited cellular complexity · Short observation periods

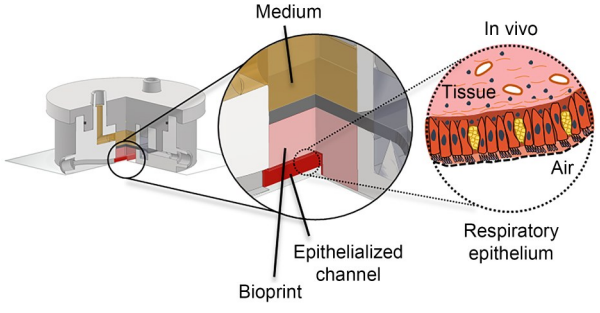

Fig. 1 Conceptualization of the engineered AoC device, featuring a channel lined with epithelial cells and stretching properties to mimic the native physiology and biomechanics of human airways. This model comprises a main culture chamber where an endothelial bioink is 3D-printed (depicted in light red, containing endothelial cells) and a perfused epithelial channel (depicted in dark red, containing respiratory epithelial cells). Both cell types are in direct contact without a physical separation such as a membrane

PDMS and other rigid polymer-based fluidic chips and membranes—limited automation, suboptimal material properties, and complex handling—were effectively addressed.

2 Methods

2.1 Chip design and fabrication

The AoC device was designed using CAD software (Autodesk Inventor Professional 2021). Figure S1a (supplementary information) illustrates the design from the top, side, and three-quarter cut views. The design was developed at a millimeter scale to maximize cultivation and analysis space while ensuring optimal accessibility for the bioprinter. The central feature of the design is the culture chamber, defined by a cubic cut-out measuring 10 mm per side and 14 mm in height, providing the primary analysis space of the chip. All inlets and outlets were formed with extruded female LUER locks to enable seamless integration with external air and media perfusion systems. Additionally, chambers with interstice tapered cubic cut-outs were subtracted from the main body of the chip to facilitate the mounting and transmission of externally applied forces onto the textile. Further mounting of the warp-knitted textile (WKT) mesh was achieved

by extruding three conical shapes at the bottom of each compression chamber to pierce the ends of the textile. The ends of the WKT were also embedded in a 1% agarose hydrogel. As shown in Fig. S1b (supplementary information), custom insertions were designed for the casting process until the embedding hydrogels were fully polymerized. To ensure a sealed flow circle, the access void was filled and sealed. A cover was designed with tapered contours matching the chambers and a slot for integrating an O-ring. All parts of the chip were 3D printed using a Stratasys Object 350 Connex3^{TM} in poly(methyl methacrylate) (PMMA; VeroClear, Stratasys, USA). After the printing process, the components underwent post-processing. All parts were manually separated from the support material (SUP705, Stratasys) and immersed in a 0.5 mol/L sodium hydroxide solution stirred at 200 r/min for 2 h. After soaking, the chambers, ports, and crevices were meticulously cleaned using forceps and needles to ensure the complete removal of the residual support material. The chip parts were then thoroughly rinsed with distilled water, dried with compressed air, and sterilized at 121 °C for 20 min.

All manufacturing experiments were conducted multiple times under the same conditions. Furthermore, the device was fabricated using a polypropylene-like material (Rigur, Stratasys), which offers durability and precision similar to PMMA. However, due to the requirement for optical transparency, this material was not considered for future studies.

2.2 Flow simulation

All simulations were conducted using COMSOL Multiphysics 6.2. Initially, a simplified 2D model was used for an exploratory study (Figs. S2–S7 in the supplementary information), followed by 3D evaluations of the selected conditions. The air and water material properties were sourced from the built-in library. Two components of the AoC—the air channel and the media chamber—were evaluated separately, focusing on shear and diffusion, respectively. Since experimental values for the gel properties were unavailable, a 2D sweep of conditions was used to examine the effects of varying gel properties and input parameters on shear and diffusion. Additional details on the 2D and 3D evaluations are provided in Figs. S2–S7 (supplementary information). The simulation aimed to determine the optimal velocities for achieving the approximate desired shear at the boundary between the air and the gel and the approximate time for the media to diffuse through the gel.

In the 3D shear evaluation, the air model was set to laminar, incompressible flow. The gel was modeled as a porous material using Darcian flow and porous slip conditions, with all other walls set to no slip. No initial values were provided, and backflow was suppressed. A 1-mm thick hydrogel was placed above the air channel. Half of the channel was evaluated with the midregion set as symmetrical, resulting in 799 487 mesh elements, ensuring a good minimum element quality of 0.1. The tested parameters included a porosity of 0.3 and permeability of 1×10^{-12} m^2 across three different velocities of 0.5, 1.5, and 2.5 m/s. Shear values were measured in the central region of the channel. Limitations in estimating shear may arise from variations in the channel geometry, such as height variations from the printed model or gel or channel width variations due to compression.

Diffusion was conducted using a laminar incompressible flow model, coupled with the transport of diluted species and mass transfer in porous media. The gel was modeled as a porous material using Darcian flow and porous slip conditions, while all other walls were set to no slip and no flux, except for inflow and outflow. Backflow was suppressed, and a stationary model was initially conducted, followed by a time-dependent model. There were no initial flow values. The inflow was set to 1 mol/m^3, which matched the initial concentration in the media chamber. The porous component started with an initial value of 0 mol/m^3. The Millington and Quirk diffusivity model was employed. A 4.3-mm thick gel was used in all evaluations. Inlet pressure was set at 2 Pa, with a porosity of 0.3, permeability of 1×10^{-12} m^2, and diffusion of 1×10^{-9} m^2/s. For the 2D model, a cross-section with 24 164 elements was used, maintaining a minimum element quality greater than 0.1. A stationary study was first conducted, followed by a time-dependent study spanning 0–24 h in 2-h intervals. The concentration at the midpoint of the chamber was analyzed. For the 3D model, half of the chamber and channels were simulated with the midregion set as symmetrical. This resulted in 2 542 229 elements, with a minimum element quality of 0.01. A stationary study was conducted first, followed by a time-dependent study (up to 2 h). Limitations in estimating media diffusion in the gel may arise from using water instead of media, which may not accurately mimic physiological processes, along with variations in gel dimensions and characteristics.

2.3 Cell isolation and culture

The L929 cell line was purchased from Sigma-Aldrich (USA), and the A549 cells were generously provided by the University Hospital RWTH Aachen. Both cell lines were expanded using standard cell culture media, comprising Dulbecco's modified Eagle medium (DMEM; Gibco, Thermo Fisher Scientific, USA) supplemented with 10% (volume fraction) fetal bovine serum (FBS; Gibco) and 1% (volume fraction) antibiotic/antimycotic solution (ABM; Gibco). For long-term storage, the cells were cryopreserved in liquid nitrogen using a freezing mixture containing 90% (volume fraction) FBS and 10% (volume fraction) dimethyl sulfoxide (DMSO; Sigma-Aldrich), which were thawed before experimental use.

Endothelial cells were isolated from the veins of fresh umbilical cords, generously provided by the Clinic for Gynecology and Obstetrics of the University Hospital RWTH Aachen. The umbilical cords were washed with phosphate-buffered saline (PBS) to remove coagulated blood, and blunt cannulas were inserted into the veins. The vein lumen was then injected with a 400 U/mL collagenase Type 1 (Sigma-Aldrich) for 30 min at 37 °C to digest the endothelium surface. The dissociated cells were then flushed away and cultured in endothelial cell growth medium-2 (EGM2; PromoCell, Germany) supplemented with 1% (volume fraction) ABM solution in flasks previously coated with a 2% gelatin solution for 30 min. The cells were frozen in liquid nitrogen using a freezing solution composed of 80% (volume fraction) DMEM, 10% (volume fraction) FBS, and 10% (volume fraction) DMSO until further use. Before bioprinting, the cells were thawed and expanded in EGM2 supplemented with 1% (volume fraction) ABM solution until Passage 5 in gelatin-coated flasks.

2.4 Preparation of embedding hydrogel and cell-laden inks

Agarose hydrogels of 1% were prepared as embedding gels by dissolving 1 g of low-gelling temperature agarose powder (Sigma-Aldrich) in 100 mL of filtered and distilled water. The gels were sterilized at 120 °C for 2 h and then cooled in an incubator at 37 °C until utilization.

To prepare the bioink, L929 or endothelial cells were washed with PBS and dissociated using a 0.05% trypsin/0.1% ethylenediaminetetraacetic acid (EDTA) solution (PAN Biotech, Germany) for 5 min at 37 °C. The dissociated cells were then counted and centrifuged. The resulting pellet was resuspended in a 10 mg/mL fibrinogen solution (Sigma-Aldrich) in tris-buffered saline (TBS; pH 7.4) to a concentration of 6×10^6 cells/mL, which will be reduced by half in the final hydrogel. The crosslinking solution was prepared with 6 U/mL thrombin (Sigma-Aldrich) and 7.5 mmol/L calcium chloride in TBS.

2.5 Assembly of the chip and bioprinting setup

A square-profiled polyamide line with a side length of 1.6 mm was cut to 80 mm and inserted through the lowest port opening, traversing the main culture chamber. A layer of light-cure adhesive (LOCTITE AA 33525, Henkel Adhesive Technologies, Germany) was applied to the underside of the base, and a polymer coverslip (ibidi, Germany) was affixed. The base was then cured under direct ultraviolet (UV) light for 5 min. A warp-knitted PET sleeve featuring a linear density of 74 dtex and a 2×1 lapping knitting structure was generously provided by the ITA Institute for Textile Technology, RWTH Aachen University. The sleeve was cut to dimensions of 10 mm×25 mm and thoroughly washed thrice using 70% ethanol and sterile PBS. Drop-on-demand (DoD) bioprinting was conducted using a bioprinter (Black Drop Biodrucker GmbH, Germany), which was used to dispense the hydrogel into the culture chamber.

Additive manufacturing technologies were also utilized to fabricate the hydrogel through bioprinting. Bioprinting is a key manufacturing technology for creating complex and heterogenic 3D cell culture systems, tissues, and organs using a layer-by-layer approach. In this study, a DoD printing strategy was selected because it provides high spatial accuracy and control during the automated dispensing of the calculated bioink, resulting in the formation of tissue structures and reproduction. The printer head was equipped with a 300-µm nozzle diameter electromagnetic microvalve (Fritz Gyger AG, Switzerland) and loaded with a 1.5-mL solution of cell-laden fibrinogen. Mounted on a three-axis robotic platform (Isel Germany AG, Germany), an air compressor (Aeolian Pixie compressor 1/6 HP max AS176; WilTec, Germany) was connected and set to 1.2 bar (1 bar= 100 kPa). The printer head was heated to 37 °C using Peltier elements. Figure S8a (supplementary information) illustrates the custom-designed CAD model of the hydrogel. The 3D model was sliced with a 0.5-mm height (Fig. S8b in the supplementary information), and drop positions (Fig. S8c in the supplementary information) were calculated using custom-built slicing software (SuperFill Software Suite 1.7, Black Drop Biodrucker GmbH). The opening time was set to 800 µs. Before the actual printing process, the coordinate origin of the printer head was referenced and later calibrated by the system and then set to its working position. A sterile PBS test print was conducted on a Petri dish to assess nozzle clogging and drop formation. The printer head was then filled with a bioink for printing.

The chip was placed in the working area of the printer head, and the sliced CAD model was printed into the primary culture chamber (Fig. S8d in the supplementary information). After each bioink printing cycle, 150 µL of the polymerizing solution was pipetted over the bioprint. After each layer, a needle was carefully inserted into the surface of the bioprint to assess layer crosslinking. After three printing cycles, the WKT was integrated. The mesh ends were inserted through the designated cut-outs using a pair of sharp forceps. Once the WKT was correctly positioned, another printing cycle was performed, followed by the application of the polymerizing solution. Each mesh end was then embedded in 250 µL of agarose hydrogel. To prevent leakage of the embedding hydrogels, custom-designed insertions were prewrapped in Teflon tape and integrated into their corresponding chambers. These insertions were removed once the agarose gel had polymerized. While the

agarose gel was semi-polymerized, three additional cycles of printing and polymerizing solution application were performed on top of the WKT. The base was left at room temperature for 5 min to allow complete gel polymerization. The chip assembly process, including printing and curing, required approximately 30–35 min. After full polymerization, the molding line was carefully extracted through one of the external ports, leaving a hollow channel within the bioprinted hydrogel.

2.6 Postprinting live/dead assay

Cell viability after printing was assessed by staining the resulting fibrin hydrogels with a 2-µmol/L calcein acetoxymethyl ester (AM) solution (Invitrogen, USA) for 20 min at 37 °C. This was followed by the addition of 2 µg/mL propidium iodide. The gel was then imaged using a two-photon laser scanning microscopy (TPLSM) Olympus FluoView 1000 MPE with a 25× water-objective NA 1.05 (Olympus Optical, Japan) and a MaiTai Deep-See Titan-Sapphire-laser (MKS Instruments, USA). Three-dimensional models with a thickness of 100 µm were generated from the resulting images and analyzed using IMARIS 9 software (Oxford Instruments, UK).

2.7 Epithelialization of the hydrogel

Endothelial cells loaded in the fibrinogen bioink were stained for 20 min at 37 °C with a 0.5% (volume fraction) dilution of the lipophilic fluorescent dye Vybrant DiO (green fluorescence, Invitrogen) in serum-free DMEM media. This was followed by three washing steps in DMEM, during which the pellet was resuspended and centrifuged consecutively. After bioprinting, the hydrogel and A549 cells were dissociated with trypsin and stained with Vybrant DiI dye (red fluorescence, Invitrogen). The stretching chip was then placed upside down, and a solution of 1×10^6 A549 cells/mL in DMEM was injected into the hollow channel of the hydrogel. The cells were left to attach to the fibrin surface for 4 h, after which the unattached cells were washed away with fresh cell culture media. The epithelialized model was incubated for an additional 24 h at 37 °C and 5% CO_2. Finally, the hydrogel was fixed with ice-cold methanol for 1 h, washed three times with PBS, and imaged using a Zeiss LSM 710 confocal laser scanning microscope. The resulting 3D stacks were processed with IMARIS 9 software (Oxford Instruments).

2.8 Stretching experiment setup

The gels were fabricated without incorporating any cells for this experiment. All samples (n=6) were analyzed as follows: an O-ring with an inner diameter of 40 mm and a thickness of 1 mm was integrated into the chip. The cover was carefully positioned to seal all remaining cavities. The inlets of the compression chambers were connected to a manual perfusion system (ibidi) with 5 mL syringes on each side. Compression and expansion of the lumen were achieved by manually injecting and withdrawing air using syringes. The perfusion system and chip were secured with tape. Images of the channel width were captured under unloaded, compressed, and expanded conditions. The channel width was then measured at equidistant positions (P=10) using image processing software (ImageJ, National Institutes of Health, USA) [26]. The compressive strain (ε_c) and tensile strain (ε_t) of the channel were calculated based on the fractional change in channel width under different stress conditions, as defined by Eq. (1):

$$\varepsilon_i = \frac{w_i - w_0}{w_0} \times 100\%. \quad (1)$$

Here, w_0 represents the unloaded channel width while w_c denotes the width after positive pressure and w_t the width after negative pressure which was applied through manual perfusion (w_i=w_c or w_t).

2.9 Statistical analysis

All statistical analyses were conducted using GraphPad Prism 9.3.1. To compare compression and tensile strains in the stretching assays, normality was assessed using the Shapiro–Wilk test, followed by a one-way analysis of variance with Tukey's post-hoc test. For the analysis of the post-bioprinting and control survival rates, the assumption of normality was also tested using the Shapiro–Wilk test, while the homogeneity of variances was confirmed with Levene's test. Both groups were then compared using an independent t-test.

3 Results and discussion

3.1 Composition and functions in the AoC design

For the design of this novel stretchable AoC, three distinct planes within the height dimensions of the base defined the functionality of the device, as demonstrated in Fig. 2. Figure 2a illustrates the media perfusion circuit and its flow concept. The media perfusion circuit was positioned at the highest level of the primary culture chamber. Fresh media were inserted through a vertical connection port and distributed over the bioprinted construct, gradually replacing the old media continuously expelled through the opposite port. The bioprint contains endothelial cells capable of

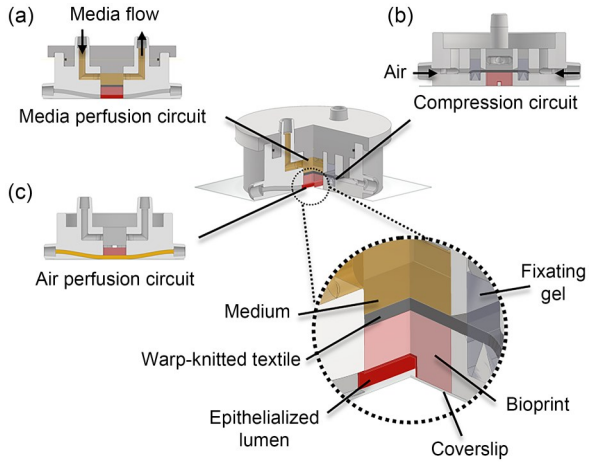

Fig. 2 Schematic representation of the AoC functions and composition, including the media perfusion circuit (a), compression circuit (b), and air perfusion circuit (c)

initiating angiogenesis during in vitro maturation cultures. Biomechanical stimuli that mimic movements during resting breathing, such as compression, expansion, and liquid-shear stress, are critical factors considered in this application. In this novel design, the compression plane was enclosed by air and cell-media perfusion circuits (Fig. 2b). Compression and expansion stimuli were applied perpendicular to and at a distance from the airway channel by stretching a WKT mesh positioned away from the cell–cell interface (depicted as a dark gray layer above the bioprint in Fig. 2b). The WKT was fixed sideways with sterile agarose hydrogel. The agarose hydrogel was selected because it can be deformed (compressed and expanded) when air pressure is applied through an external air pump. The lower section of the device was dedicated to air perfusion, mimicking the apical side of the ALI in the main chamber. Figure 2c outlines the concept, where a squared profiled lumen is formed within the cell-containing hydrogel by inserting a polyamide molding line before bioprinting, which was later removed after polymerization. This resulting lumen facilitates epithelialization as an object-free cell interface.

All three components of the AoC were fabricated using 3D printing. A significant advantage of this approach is its ability to seamlessly integrate complex functional structures into the base design across multiple working planes in a single manufacturing step. Moreover, this manufacturing method enables the use of PMMA, which is inherently impermeable to small molecules, making it more suitable for molecular and drug assays than standard PDMS [27]. PMMA, particularly the VeroClear variant, offers excellent strength and stiffness, making it ideal for translating compression movements without compromising structural integrity. Additionally, clear acrylic is an alternative to glass, enabling the visualization of internal components and features. The transparency properties of PMMA also facilitate real-time monitoring during the bioprinting process. By simplifying production and reducing costs, 3D printing enhances manufacturing efficiency. Overall, the AoC design effectively incorporates all the essential characteristics of a dynamic fluidic chip, including the ability to mimic biomechanical stimuli in the airway and support the perfusion of air and media.

3.2 Analysis of AoC fabrication quality and design features

Figure 3a illustrates the AoC in its pre-processed, post-processed, and final states. During 3D printing, supporting material was incorporated to reinforce overhanging, bridging, and complex, fragile structures. This approach allows all conceptualized functions to be fabricated in a single process while ensuring structural stability. In the design phase, all components were designed on a millimeter scale, with joint tolerance set at 0.5 mm to account for potential deviations during fabrication. While the fabricated chip closely aligned with its original design, minor discrepancies were observed due to printing inaccuracies. Figure 3b highlights the major fabrication defects, particularly in the compression chambers and airway channel, compared to the original designs. These defects were addressed during device assembly by strategically placing supporting gels in the respective chambers and securing the cover slide at the base of the chip without compromising functionality. Although the cones within the compression chambers exhibited a slight reduction in sharpness, the WKT was successfully mounted and fixed using agarose hydrogel. The design of the airway channel adhered to a specific approach, ensuring that the

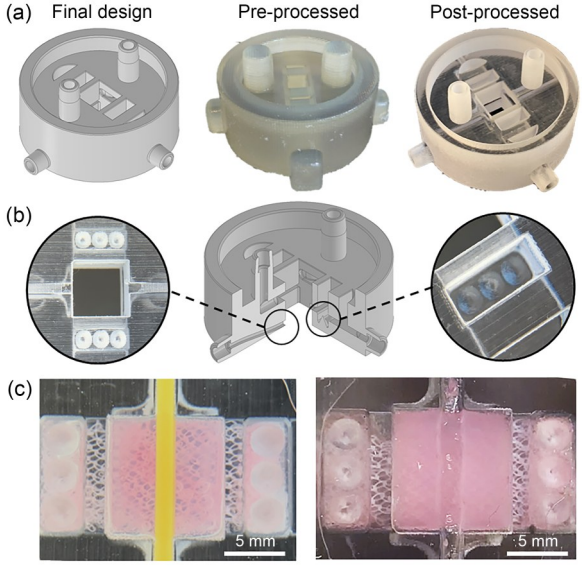

Fig. 3 Illustrations of the AoC fabrication: (a) fabrication process; (b) major fabrication defects; (c) images showing the lumen casting process after the full assembly of the AoC

molding object maintained continuous contact with the coverslip. To achieve this, a squared profile along a spline with six symmetrical, equidistant control vertices was subtracted from the body of the chip during the design phase. However, the wall thickness linearly decreased toward the main chamber, making precise printing of this structure challenging. This limitation was addressed by utilizing a light-hardened adhesive to attach a polymer slide to the bottom of the chip. Consequently, the slide offered segments with a thinner wall thickness for airway channel support, effectively sealing the boundary points between the channel and the main chamber. As previously conceptualized and illustrated in Fig. 3c, the molding object runs through the bioprint in the primary chamber, maintaining constant contact with the upper side of the polymer slide. Figure 3c shows a successfully cast lumen at the bottom of the primary chamber after removing the molding object following bioprint polymerization. Additionally, the squared profile of the lumen allows for real-time visual analyses (e.g., through various types of microscopy) of the epithelial layer at the ALI from below.

A minimalistic design approach was adopted to reduce complexity and enhance control during subsequent handling and operation [4]. All design decisions were guided by the fundamental principles of sound engineering and insights gained from previous in vitro setups [28]. The system is designed to be easily operated by users familiar with standard cell culture practices, requiring minimal training, making it suitable for both academic and commercial use. While some of our team members with limited cell culture experience have successfully used the system, further refinements could enhance the user experience in future studies. The design was developed on a millimeter scale, ensuring compatibility with the bioprinter and enabling a stable 3D printing process. The initially conceived complex design features and functions were successfully translated into a manufactured final product. Throughout this process, minor fabrication differences were addressed and adjusted accordingly.

Compared to traditional testing methods, fluidic chips offer the advantage of allowing optical real-time analyses. However, the limited optical transparency of certain 3D-printing polymers restricts the widespread application of 3D-printed chips in imaging-based in vitro testing [4]. Additionally, the transparency of the hydrogel may affect the visibility of the ALI. The AoC described here enables optical real-time monitoring of the ALI in both the chip and hydrogel components. This special feature was achieved through meticulous material placement, lumen design within the chip and bioprint, and a cell-coating process applied to the lumen. This novel chip design introduces new possibilities for utilizing various materials in fabricating 3D-printed chips. Consequently, this concept simplifies fabrication processes, increases the accessibility of AoCs, and ultimately improves the efficiency of drug assays while reducing associated costs. Unlike other currently available AoCs that often rely on a PDMS membrane at the cell interface, this novel concept employs PDMS-free fabrication throughout the entire chip. The absence of barriers and PDMS at the cell interface improves cell−cell interactions and more accurately mimics native tissue characteristics with greater authenticity.

3.3 Simulation of airflow and medium in the AoC

An *in silico* simulation study was conducted to determine the velocities required to achieve the approximate desired shear at the boundary between air and gel (Fig. 4a) and to estimate the time needed for media diffusion through the AoC gel. Shear stress caused by airflow at the boundary of the gel within the air channel was assessed (Fig. 4b). Various parameters (Figs. S2–S5 in the supplementary information) were considered to approximate a bronchi shear stress range of 0.1–0.4 Pa [29]. For the proposed model, a velocity of 1.5 m/s at the inlet point achieves the desired shear stress (Figs. 4c and 4d). To ensure uniform shear stress across the entire surface, a velocity of 1.2 m/s produces shear stress ranging from 0.13 to 0.39 Pa along the width and length of the channel.

An *in silico* diffusion analysis was conducted to estimate the minimum time required for the media in the chamber to reach the cells within the gel (Fig. 5). Various parameters (Figs. S6 and S7 in the supplementary information) were considered to model media diffusion (Figs. 5a–5c). For simplification, water was simulated instead of media. In the proposed model, with an inlet pressure of 2 Pa, the media are expected to reach the bottom of the gel within 2 h, with likely complete diffusion by 6 h (Fig. 5c).

3.4 Cell viability postprinting and channel epithelialization

A fibrinogen-based bioink containing L929 fibroblasts was deposited within the main chamber of the chip using a DoD bioprinter (Fig. 6a), followed by the addition of a thrombin crosslinking solution. L929 fibroblasts were selected for viability assays based on ISO 10993 guidelines for the biological evaluation of medical devices. The printing procedure subjects cells to significant shear stress, necessitating a postprinting analysis of cell survival rates. For this purpose, the cells embedded in the bioink were stained with calcein AM to label living cells in green and propidium iodide to label dead cells in red (Fig. 6b). TPLSM was used to visualize the staining, resulting in a post-bioprinting survival rate of (86±4.1)% compared to (93±0.9)% in the control

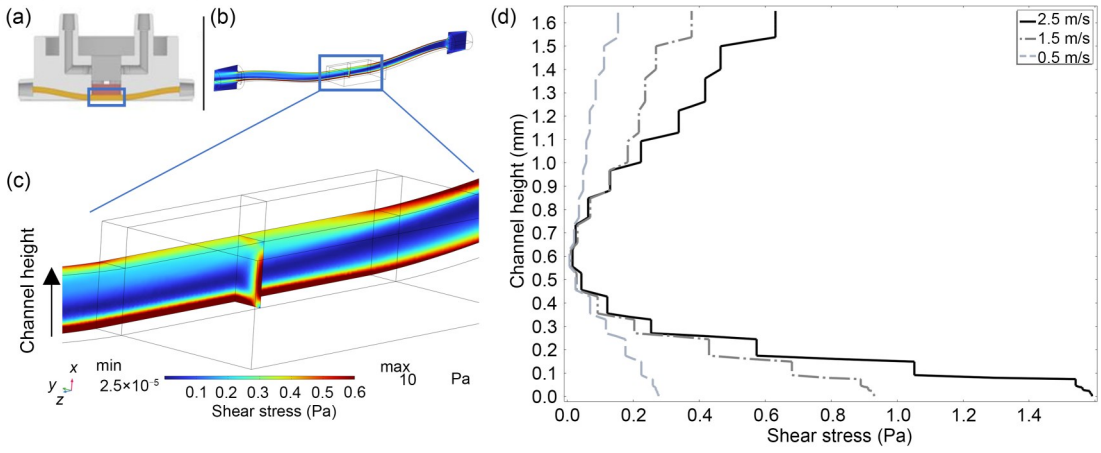

Fig. 4 Simulation of shear stress in the air channel of the AoC. (a) Cross-section highlighting the air channel and region of interest. (b, c) Three-dimensional heat map showing shear stress along the air channel and at the region of interest at a velocity of 1.5 m/s. The heat map was capped at a maximum of 0.6 Pa for better visualization of the shear stress at the top surface of the air channel. (d) Shear stress evaluation for different velocities (0.5, 1.5, and 2.5 m/s) at the midregion of the channel plotted against the height of the channel. The inlet flow is from right to left. All conditions include the following inputs: porosity=0.3 and permeability=1×10^{-12} m^2

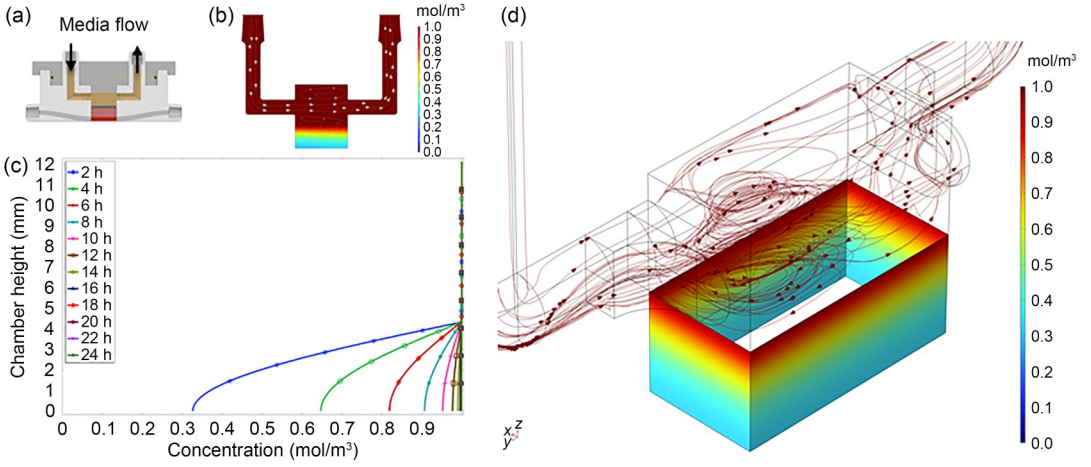

Fig. 5 Simulation of the media channel in the AoC. (a) Cross-section highlighting the media channel. (b) Two-dimensional cross-section model showing water diffusion at 2 h. (c) The concentration of water diffusing through a 2D hydrogel model at the central region of the chamber over time. (d) Three-dimensional heat map illustrating diffusion streamlines and surface flux at 2 h. The input conditions include pressure=2 Pa, porosity=0.3, permeability=1×10^{-12} m^2, and diffusion=1×10^{-9} m^2/s. The inlet flow is from left to right

samples (Fig. 6c). Therefore, the effect of bioprinting on cell survival is minimal, as it was not statistically significantly lower than the nonprinted samples.

Removing the molding line created an internal channel within the bioprinted fibrin hydrogel (Fig. 3c). To assess the capacity to convert this channel into a respiratory passage model, A549 lung epithelial cells were injected into the channel and allowed to adhere. In this experiment, the fibrin bioink was loaded with endothelial cells to mimic the highly vascularized lung mucosa. The visualization of the model demonstrates the ability of epithelial cells to attach to the channel (Figs. 6d and 6e).

These results highlight the capacity of the chip to support a bioprinted respiratory model. Unlike most current stretchable AoC models, which consist of dual 2D cell layers mimicking the epithelial–endothelial interface on both sides of a synthetic membrane [30, 31], our chip facilitates combining different cell types with mechanical stimulation. It allows for direct cell–cell interactions and free migration within a 3D matrix. Future studies may build upon this proof-of-concept chip design, for example, to conduct long-term experiments for tissue maturation with a fully differentiated epithelium that more closely mimics native tissue function. Varying stretching rates and speeds would allow for an in-depth study of airway biomechanics in health and disease. Additionally, other cell types, such as perivascular cells, could be incorporated to promote the development of an interconnected network of vessels, thus enabling perfusion with bioactive agents or drugs [25].

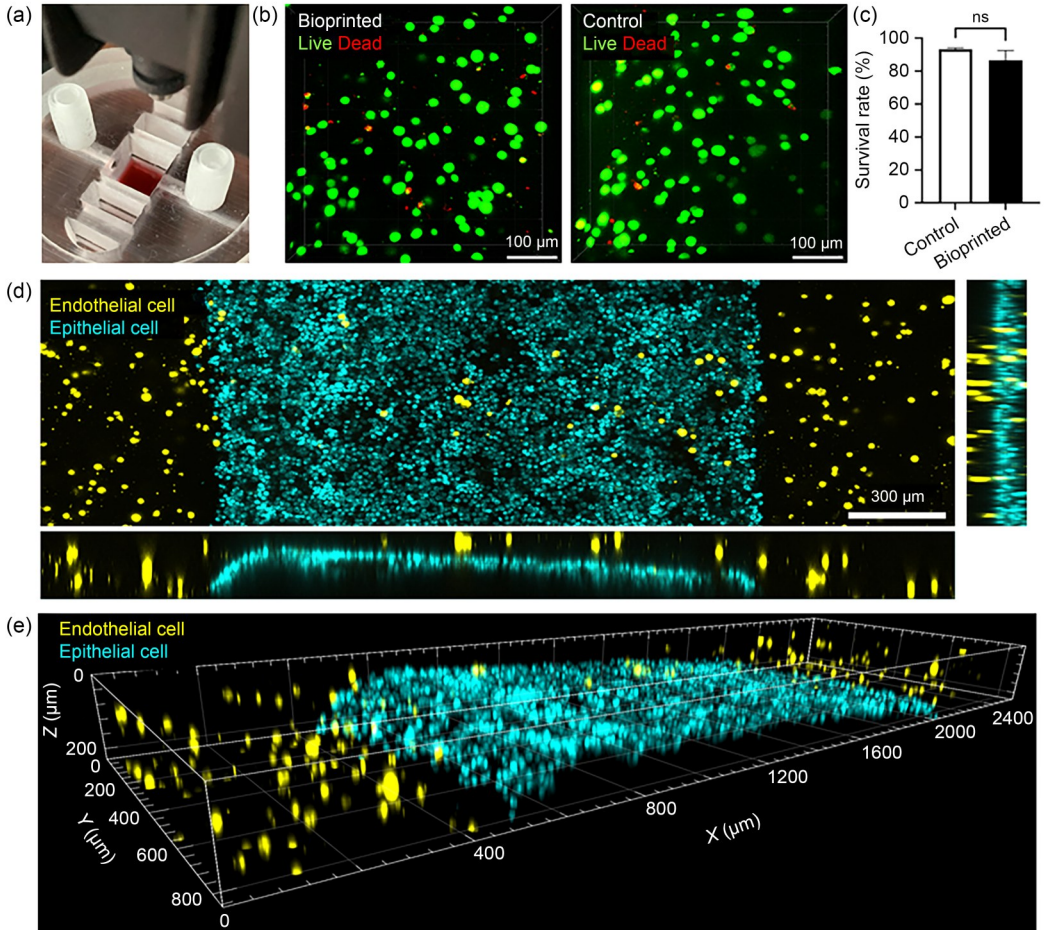

Fig. 6 Cell viability postprinting and channel epithelialization. (a) DoD bioprinting within the main stretching chip chamber. (b) Representative images from two-photon laser scanning microscopy *Z*-stacks of bioprinted and control samples after calcein AM and propidium iodide staining (green: living cell; red: dead cell). (c) Statistical analysis of the live/dead assay after printing did not show significant differences (data are expressed as mean±standard deviation; n=3, using Student's t-test). (d) Top view and cross-sections of the endothelial cells embedded in the fibrin hydrogel (yellow) surrounding the internal channel coated with epithelial cells (blue). Both cell types were stained with lipophilic, nontoxic dyes for confocal microscopy imaging. (e) Three-dimensional projection of the model with a thickness of 200 µm

3.5 Evaluation of the stretching capacity of the AoC device

Compression and tension strains in the airway lumen were assessed by imaging the response of the lumen under three distinct conditions—unloaded, compressed, and expanded. These conditions within the lumen were achieved by attaching the AoC to a perfusion system with 5 mL syringes, as shown in Fig. 7a. Compression and tensile strains in the lumen were induced through manual injection and evacuation of air. In image processing, as shown in Fig. 7b, 10 equidistant positions (P=10) along the axis of the lumen were defined. At each position (n=6) of the specimen, the channel width was measured under varying stress levels. Compression and tensile strains were calculated based on the fractional change in width. Figure 7c illustrates the average compression and tensile rates at each position. Therefore, compression rates varied from −14.7% to −5.2%, while tensile rates ranged from 2.0% to 6.4%. When averaged across all defined positions in the lumen, the compression rate was −10.0% and the tensile rate was 4.5%.

Biomechanical stimuli are a critical aspect of any on-chip application and are essential for mimicking the behavior of native tissue. Mechanical stimuli not only influence cell behavior and tissue development but also impact disease status and drug responsiveness [14]. Standard fluidic devices lack the capacity for realistic stretching motions to mimic an airway profile. Conventional AoCs utilize an unfavorable PDMS membrane in the cell interface to achieve stretch. In this study, the interface movements were achieved by applying pneumatic stress to an embedded WKT positioned distant from the cell–cell interface. The strain experiments yielded comparable compression and tensile strain rates across positions 3–9 and 5–8, respectively. Despite implementing measures during the design to diffuse

the compression air inflow and create a homogenous flow field, preferential flow directed toward positions 5 and 6 was detected. This phenomenon is illustrated in Fig. 7c, where stable performance in both compression and tensile strains was observed across all specimens. Further comparisons and analyses were conducted based on these optimal positions. In vivo, the mechanical strain experienced in the airway ranges from 5% to 15% in linear dimensions [32, 33]. Interestingly, these rates align with the results obtained for the developed device at its optimal positions (5 and 6). Specifically, an average compression strain of −13.1% was achieved, along with a corresponding tensile strain of 5.1% at these positions. This validates that the developed AoC can effectively mimic the physiological strain within the desired range in its optimal positions. Notably, existing PDMS membrane AoCs achieve a minimum strain rate of 5% [11, 12], which can be achieved in the presented AoC at Positions 2, 5, 6, 8, and 10.

Although the stretching capacity was tested using manual injection, this proof-of-concept chip can be easily integrated with an automated perfusion system or pump. Future studies will focus on enhancing the complexity of this model both biologically and mechanically, as well as automating the pre- and postprinting processes as extensively as possible.

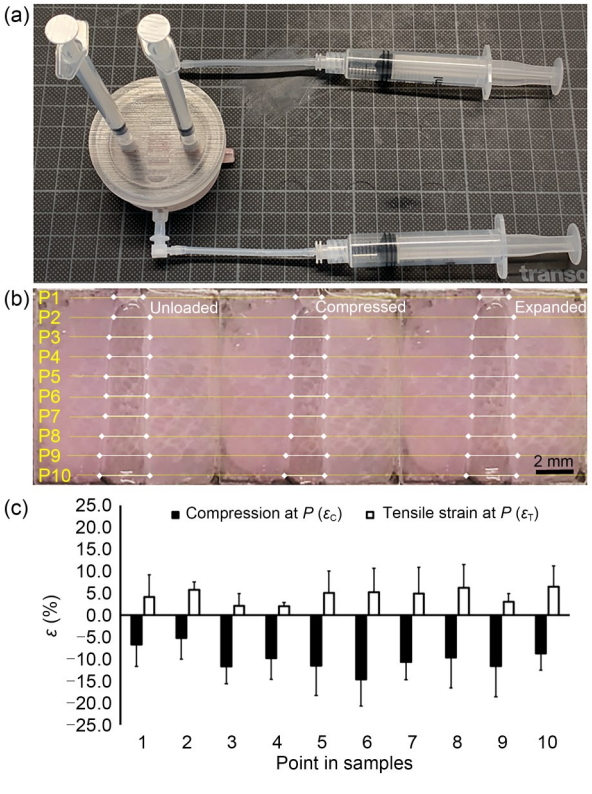

Fig. 7 Stretching capacity of the AoC device. (a) Illustration of the strain experiment setup. (b) Division of the cast lumen into equidistant positions with channel width measurements in unloaded, compressed, and expanded conditions. (c) Illustration of the average compression and tensile strains across Positions 1–10 (data are expressed as mean±standard deviation; n=6)

4 Conclusions

The 3D printing of thermoplastics was utilized to biofabricate an AoC model. This approach offers an alternative to traditional manufacturing methods, such as lithography and PDMS molding. Due to their biocompatibility, affordability, widespread availability, and ease of fabrication, thermoplastics are an attractive material choice for fabricating fluidic devices. To enhance automation and replication rates in the on-chip system and accurately mimic tissue structures, a DoD bioprinting strategy was employed to fabricate the in vitro airway model. In this study, we introduced a novel approach for emulating tissue composition accuracy by creating a membrane-free contracting cell interface. Unlike the traditional AoC models, where a polymer membrane dominates the ALI, this design replaces the membrane with a WKT, integrated distant from the cell–cell interface. The newly designed model presented in this study has shown mechanical stimulation and dynamic fluid flow that mimics native airways—an achievement not seen in state-of-the-art models. The selected design enhanced optical accessibility, allowing real-time monitoring of both bioprinting and cell–cell interface postprinting. Nonetheless, this AoC model is still in the early stage of development and could benefit from long-term follow-up studies with greater biological complexity. In summary, we have shown that an engineered stretchable AoC could be fabricated, potentially serving as a suitable alternative to the state-of-the-art in vivo and in vitro models for the future testing of therapies, such as those for airborne diseases.

Supplementary Information The online version contains supplementary material available at https://doi.org/10.1631/bdm.2400351.

Acknowledgements The authors would like to thank the Department of Gynecology and Perinatal Medicine (Prof. Stickeler) for providing the umbilical cords. This work was supported by the Core Facility Two-Photon Imaging Facility and the Confocal Microscopy Facility, both parts of the Interdisciplinary Centre for Clinical Research (IZKF) of the Faculty of Medicine at RWTH Aachen University. This study was supported by the Volkswagen Foundation (Grant No. Az 99078 to DDC, ALT, and MT). This research was funded by the Deutsche Forschungsgemeinschaft (DFG, German Research Foundation) under Germany's Excellence Strategy–2082/1–390761711 (to DDC) and as part of the research training group GRK 2415–Mechanobiology in Epithelial 3D Tissue Constructs (project number 363055819, to ALT and SJ).

Author contributions All authors contributed to the study conception and design. Material preparation and data collection and analysis were performed by JC, JGR, OODLJ, and YV. The first draft of the manuscript was written by JC, JGR, and DDC, and all authors commented on previous versions of the manuscript. All authors read and approved the final manuscript.

Funding Open access funding enabled and organized by DEAL.

Declarations

Conflict of interest The authors declare that they have no conflict of interest.

Ethical approval This article does not contain any studies with human or animal subjects performed by any of the authors. Umbilical cords were provided by the Centralized Biomaterial Bank of the RWTH Aachen University (cBMB) according to its regulations, following RWTH Aachen University Medical Faculty Ethics Committee (cBMB project number 323) after informed consent.

Data availability The data that support the findings of this study are available from the corresponding author upon reasonable request.

References

1. Zhang BY, Radisic M (2017) Organ-on-a-chip devices advance to market. Lab Chip 17(14):2395–2420. https://doi.org/10.1039/c6lc01554a
2. McGonigle P, Ruggeri B (2014) Animal models of human disease: challenges in enabling translation. Biochem Pharmacol 87(1):162–171. https://doi.org/10.1016/j.bcp.2013.08.006
3. Bhise NS, Ribas J, Manoharan V et al (2014) Organ-on-a-chip platforms for studying drug delivery systems. J Contr Release 190:82–93. https://doi.org/10.1016/j.jconrel.2014.05.004
4. Leung CM, de Hann P, Ronaldson-Bouchard K et al (2022) A guide to the organ-on-a-chip. Nat Rev Methods Primers 2:33. https://doi.org/10.1038/s43586-022-00118-6
5. Whitesides GM (2006) The origins and the future of microfluidics. Nature 442:368–373. https://doi.org/10.1038/nature05058
6. Kim S, Takayama S (2015) Organ-on-a-chip and the kidney. Kidney Res Clin Pract 34(3):165–169. https://doi.org/10.1016/j.krcp.2015.08.001
7. Skommer J, Wlodkowic D (2015) Successes and future outlook for microfluidics-based cardiovascular drug discovery. Expert Opin Drug Discov 10(3):231–244. https://doi.org/10.1517/17460441.2015.1001736
8. Mastrangeli M, Millet S, Orchid Partners T et al (2019) Organ-on-chip in development: towards a roadmap for organs-on-chip. Altex 36(4):650–668. https://doi.org/10.14573/altex.1908271
9. Bhatia SN, Ingber DE (2014) Microfluidic organs-on-chips. Nat Biotechnol 32:760–772. https://doi.org/10.1038/nbt.2989
10. Bennet TJ, Randhawa A, Hua J et al (2021) Airway-on-a-chip: designs and applications for lung repair and disease. Cells 10(7): 1602. https://doi.org/10.3390/cells10071602
11. Nawroth JC, Roth D, van Schadewijk A et al (2023) Breathing on chip: dynamic flow and stretch accelerate mucociliary maturation of airway epithelium in vitro. Mater Today Bio 21:100713. https://doi.org/10.1016/j.mtbio.2023.100713
12. Huh D, Matthews BD, Mammoto A et al (2010) Reconstituting organ-level lung functions on a chip. Science 328(5986):1662–1668. https://doi.org/10.1126/science.1188302
13. Ingber DE (2006) Cellular mechanotransduction: putting all the pieces together again. FASEB J 20(7):811–827. https://doi.org/10.1096/fj.05-5424rev
14. Thompson CL, Fu S, Heywood HK et al (2020) Mechanical stimulation: a crucial element of organ-on-chip models. Front Bioeng Biotechnol 8:602646. https://doi.org/10.3389/fbioe.2020.602646
15. Weisgrab G, Ovsianikov A, Costa PF (2019) Functional 3D printing for microfluidic chips. Adv Mater Technol 4(10): 1900275. https://doi.org/10.1002/admt.201900275
16. Corral-Nájera K, Chauhan G, Serna-Saldívar SO et al (2023) Polymeric and biological membranes for organ-on-a-chip devices. Microsyst Nanoeng 9:107. https://doi.org/10.1038/s41378-023-00579-z
17. Amin R, Knowlton S, Hart A et al (2016) 3D-printed microfluidic devices. Biofabrication 8(2):022001. https://doi.org/10.1088/1758-5090/8/2/022001
18. Radisic M, Loskill P (2021) Beyond PDMS and membranes: new materials for organ-on-a-chip devices. ACS Biomater Sci Eng 7(7):2861–2863. https://doi.org/10.1021/acsbiomaterials.1c00831
19. Toepke MW, Beebe DJ (2006) PDMS absorption of small molecules and consequences in microfluidic applications. Lab Chip 6:1484–1486. https://doi.org/10.1039/B612140C
20. Halldorsson S, Lucumi E, Gómez-Sjöberg R et al (2015) Advantages and challenges of microfluidic cell culture in polydimethylsiloxane devices. Biosens Bioelectron 63:218–231. https://doi.org/10.1016/j.bios.2014.07.029
21. Carvalho MR, Lima D, Reis RL et al (2015) Evaluating biomaterial- and microfluidic-based 3D tumor models. Trends Biotechnol 33(11):667–678. https://doi.org/10.1016/j.tibtech.2015.09.009
22. Nawroth J, Senger C, Roth D et al (2021) A modular human airway lung-chip for studying the effect of breathing-mechanics on airway epithelial cell biology. FASEB J 35(S1). https://doi.org/10.1096/fasebj.2021.35.S1.00381
23. Sakolish C, Georgescu A, Huh DD et al (2022) A model of human small airway on a chip for studies of subacute effects of inhalation toxicants. Toxicol Sci 187(2):267–278. https://doi.org/10.1093/toxsci/kfac036
24. Zhu YJ, Sun LY, Wang Y et al (2022) A biomimetic human lung-on-a-chip with colorful display of microphysiological breath. Adv Mater 34:2108972. https://doi.org/10.1002/adma.202108972
25. Park S, Newton J, Hidjir T et al (2023) Bidirectional airflow in lung airway-on-a-chip with matrix-derived membrane elicits epithelial glycocalyx formation. Lab Chip 23:3671–3682. https://doi.org/10.1039/D3LC00259D
26. Schneider CA, Rasband WS, Eliceiri KW (2012) NIH Image to ImageJ: 25 years of image analysis. Nat Methods 9(7):671–675. https://doi.org/10.1038/nmeth.2089

27. Ali U, Karim KJBA, Buang NA et al (2015) A review of the properties and applications of poly (methyl methacrylate) (PMMA). Polym Rev 55(4):678–705. https://doi.org/10.1080/15583724.2015.1031377
28. Bahill AT, Botta R (2008) Fundamental principles of good system design. Eng Manag J 20(4):9–17. https://doi.org/10.1080/10429247.2008.11431783
29. Koombua K, Pidaparti RM (2008) Inhalation induced stresses and flow characteristics in human airways through fluid-structure interaction analysis. Model Simul Eng 2008(1):358748. https://doi.org/10.1155/2008/358748
30. Sisodia Y, Shah K, Sayyed AA et al (2023) Lung-on-chip microdevices to foster pulmonary drug discovery. Biomater Sci 11(3):777–790. https://doi.org/10.1039/D2BM00951J
31. Tavares-Negrete JA, Das P, Najafikhoshnoo S et al (2023) Recent advances in lung-on-a-chip technology for modeling respiratory disease. Bio-Des Manuf 6:563–585. https://doi.org/ 10.1007/s42242-023-00241-7
32. Khangure SR, Noble PB, Sharma A et al (2004) Cyclical elongation regulates contractile responses of isolated airways. J Appl Physiol 97(3):913–919. https://doi.org/10.1152/japplphysiol.00262.2004
33. LaPrad AS, Lutchen KR, Suki B (2013) A mechanical design principle for tissue structure and function in the airway tree. Plos Comput Biol 9(5):e1003083. https://doi.org/10.1371/journal.pcbi.1003083